Journal of Thermal Analysis and Calorimetry, Vol. 69 (2002) 371–385

DESIGN AND DEVELOPMENT IN SELF-REFERENCE DIFFERENTIAL SCANNING CALORIMETRY*

*B. J. Holland, J. R. Atkinson and J. N. Hay***

School of Metallurgy & Materials, The University of Birmingham, Edgbaston, Birmingham B15 2TT, UK

(Received June 10, 2001)

Abstract

An intermediate range (50–1000°C) self-referencing differential scanning calorimeter (SR-DSC) has been built and its performance evaluated. The SR-DSC measures heat flow across a heat flow metal plate, and any changes to the heat flow caused by a thermal transition occurring in a centrally placed sample is monitored by a temperature difference across the plate. The criteria for high sensitivity are that the circular plate should be as thin as possible and have a low thermal conductivity. The best sensitivity conducive with robust behaviour was achieved with an inconel thermal plate of uniform thickness, 75 μm, this gave reproducible results, and the enthalpy of the thermal transition was proportional to sample mass. Calorimeter sensitivity decreased with increasing temperature and a sloped baseline was observed. Both of these effects can be corrected mathematically. An example of the use of the SR-DSC in polymer characterisation was limited to a study of the physical ageing of PET.

Keywords: self-referencing differential scanning calorimetry, thermal conductivity

Introduction

This paper is concerned with the design and development of a high quality, medium range temperature (50–1000°C), low-cost self-referencing differential scanning calorimeter (SR-DSC) for use in industrial characterisation and materials research, and an evaluation of its performance characteristics. As part of this investigation finite element analysis of the heat flow characteristics of SR-DSC thermal plates was carried out, in order to determine the effect of plate material, thickness and geometry on calorimeter performance.

Currently, there are two widely used designs of DSC – heat flux [1] and power compensation [2]. Heat flux DSC measures the temperature difference between two cells placed symmetrically in a furnace, one containing the sample and the other a reference material, as a function of reference temperature. During a thermal transition,

* Paper was read at the TAC2001 Conference in Liverpool

** Author for correspondence: E-mail: j.n.hay@bham.ac.uk

1418–2874/2002/ $ 5.00

Akadémiai Kiadó, Budapest
Kluwer Academic Publishers, Dordrecht

the temperature difference between the sample and reference will produce a signal proportional to the thermal response of the transition. The main advantage of heat flux DSC is the simplicity of the design, but the disadvantages are the difficulty in producing exact symmetry between the sample and reference cells. The reference material is usually assumed to have negligible heat capacity and thermal conductivity, and usually this is achieved by encapsulating the sample in an aluminium pan, and using an identical aluminium pan as the reference material. A sloped baseline is always observed. In addition, heat flux DSC's often require a long time period to return to equilibrium following a thermal transition, leading to impaired resolution.

Power-compensated DSC operates by adjusting the power supplied to sample and reference cells, in order that the temperature of both is equal and follows a predetermined temperature program. During a thermal transition, a signal is produced according to whether more or less power is required to keep the temperature of the sample cell consistent with that of the reference. The DSC curves produced are similar to those produced in heat flux DSC, but are compressed in time according to the swiftness of the heater control, giving improved resolution.

SR-DSC measures heat flow across a circular plate, placed within a circular furnace, in the uniform part of the furnace. Thermocouples were placed centrally beneath the sample, and at four reference positions at a predetermined distance between the furnace walls and the centre of the plate. The SR-DSC has a single, centrally placed sample, but unlike conventional DSC designs has no reference, the absence of which nullifies baseline inconsistencies caused by calorimeter asymmetry, and thermal noise at the reference-plate interface.

Experimental

Tubular furnaces of internal diameter 21 mm made from silver, copper and stainless steel, were wound with insulated nichrome furnace wire (1 mm outer diameter) capable of operating up to 1000°C, supplied by Thermocoax. Power was supplied by a computer controlled thyristor. A K type thermocouple embedded in the furnace wall was used to provide the temperature feedback to control.

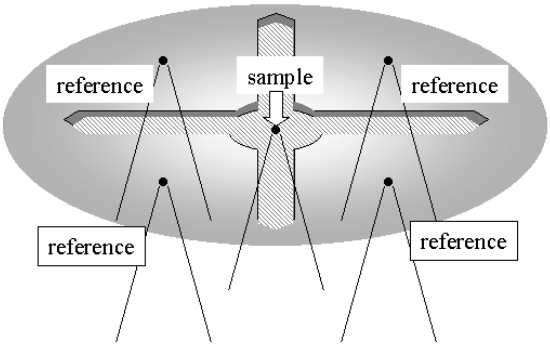

Fig. 1 SR-DSC plate

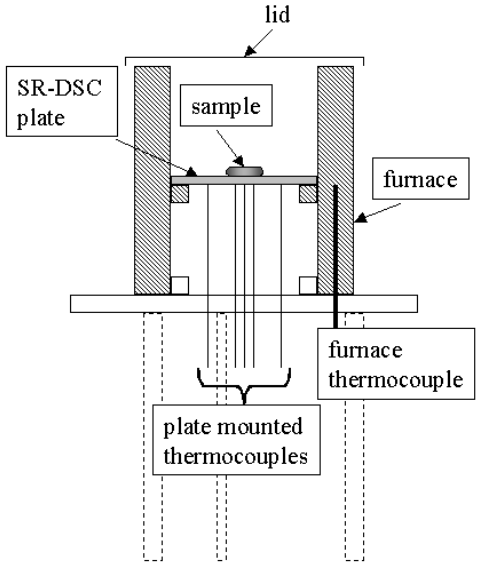

Fig. 2 Schematic diagram of SR-DSC

SR-DSC heat flow plates, (Fig. 1), were stamped from thin metal foils (of thickness up to 200 μm), and contained a circular, centrally placed sample recess (6 mm diameter), and shallow ridges to provide structural rigidity. K type thermocouples (0.25 mm diameter) were spot welded to the underside of the plate, four reference thermocouples were placed 6 mm from the centre of the plate, and a single sample thermocouple was placed beneath the central sample area. The average reference temperature is subtracted from the sample temperature to provide a signal.

The plate is rested on a ledge in the middle of the furnace, and the thermocouple wires fed out though narrow ceramic tubes in the bottom of the furnace. A removable cover protects the sample area. The furnace was supported on a tripod inside an aluminium environmental chamber (Fig. 2). The SR-DSC furnace was controlled by an IBM compatible computer using a high-performance data acquisition card (National Instruments PCI-MIO-16XE), which was also used to collect sample and reference thermocouple readings. The thermocouples were connected to the data acquisition card via a signal-conditioning accessory. Software to control the furnace and collect data was written in-house using Labview 5.1.

Thin sheets of nickel, constantan, silver and inconel 600 of thickness 50–200 μm, used to produce thermal plates, were supplied by Goodfellow Cambridge Ltd.
Highly pure metal samples were used to calibrate and characterise the instrument. Indium (99.999% pure) was supplied by Koch–Light Laboratories Ltd, England. Tin (99.999% pure), lead (99.999% pure) and zinc (99.999% pure) was supplied by Fluka AG, Switzerland. The poly(ethylene terephthalate) (PET) used in this study was DuPont Melinar, which could be converted to the amorphous form by cooling from the melt on an aluminium surface.

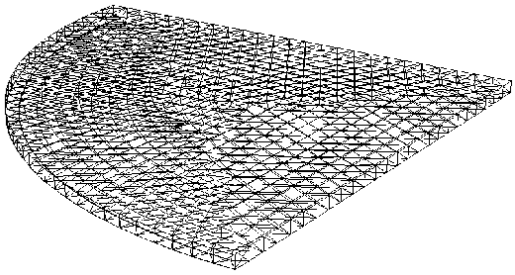

Fig. 3 Diagram of meshed plate

As part of this investigation, Finite Element Analysis (FEA) was used to model SR-DSC thermal plate behaviour, and the effect of material choice, thickness and geometry. FEA was carried out using Abaqus CAE software (Hibbitt, Karlsson & Sorensen Inc.). To simplify the process, calculations were performed on sections representative of one quarter of a plate. The model was meshed using an in-built meshing algorithm, using four-node linear heat transfer tetrahedron elements (Fig. 3). In order to simulate heating of the plate, a boundary condition was applied to the edge of

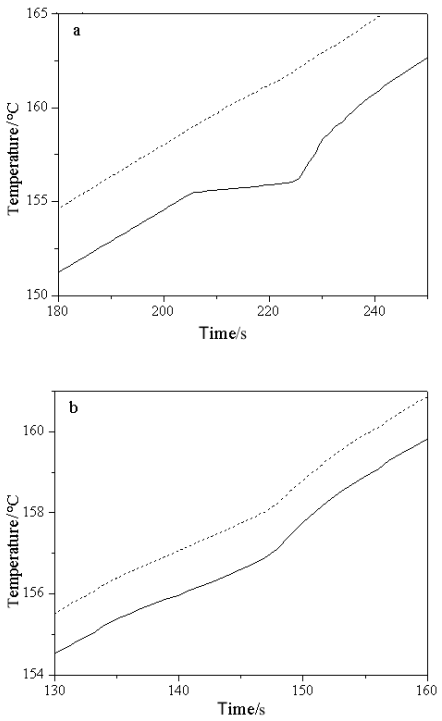

Fig. 4 Thermocouple cross-talk, a – sample, in a 75 micron inconel plate —, b – reference, in a 100 micron silver plate ·····

the plate. The magnitude of the boundary condition was equal to the final temperature required, and was defined to increase linearly with time. Simulations of the heat flow characteristics of several plates were investigated, and the preliminary results are presented.

Results and discussion

The temperature of the furnace was controlled by the use of a proportional-integral-derivative (PID) feedback loop, which was embedded into the data acquisition software. The PID values were calculated using an auto-tune algorithm, and once this had been achieved, the furnaces displayed excellent control (±0.05°C) both in dynamic and isothermal modes. Silver melts at 960°C, which excludes its use at high temperatures, whilst the copper furnace underwent severe oxidation in air above 400°C. Meanwhile, operation of the stainless steel furnace above 500°C showed only minor surface discolouration, and was capable of 1000°C without melting. For this reason the stainless steel furnace was chosen for this application.

The initial concern was that there could be some 'cross-talk' between sample and reference thermocouples due to their close proximity on the plate. Figure 4 shows the behaviour of sample and reference thermocouples during the melting of 10 mg of indium on 75 mm inconel (Fig. 4a) and 100 mm silver plates (Fig. 4b), using a heating rate of 10°C min^{-1}. It was found that for inconel, constantan and nickel plates, the temperature of the reference thermocouple reading did not deviate from the heating rate during the melting process. For inconel, the results indicate that provided there was a distance of 6 mm between sample and reference thermocouples, no cross-talk occurred. In the case of silver, where the thermal conductivity is much higher, heat from the reference thermocouple area of the plate can easily be passed to the sample, and some cross-talk was found to occur (Fig. 4b).

Table 1 Variation of thermal conductivity with temperature of selected materials [3]

Material	Thermal conductivity / W m^{-1} K^{-1} at various temperatures			
	300 K	400 K	600 K	800 K
Inconel	11.7	13.5	17.0	20.5
Constantan	23.0	–	–	–
Nickel	90.7	80.2	65.6	67.6
Silver	429	425	412	396

The reproducibility of SR-DSC was found to be excellent for all the plates tested, with area measurements reproducible to within an error margin of about 3%. Figure 5 shows three DSC traces obtained by melting 10 mg of indium on a 75 μm inconel plate, and demonstrates the extent to which the results are reproducible.

SR-DSC curves were obtained for the melting of indium, tin, lead and zinc at masses of 1, 5 and 10 mg on inconel plates. The results of the calibration of the 75 μm

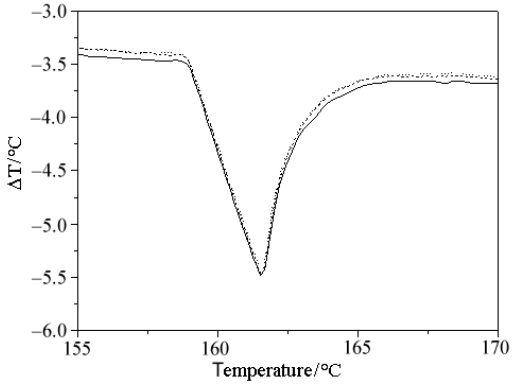

Fig. 5 Evaluation of reproducibility of SR-DSC results by melting 10 mg of indium on a 75 micron inconel plate

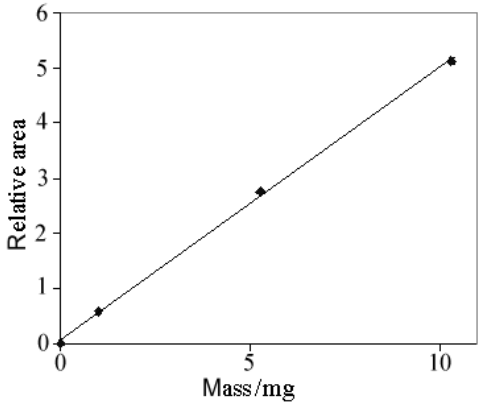

Fig. 6 Indium mass calibration for 75 micron inconel plate

inconel plate were linear and are shown in Fig. 6. for indium. The slope of the calibration plot can be used to calibrate the heat flow axis (y-axis), as will be shown.

The sensitivities of the inconel plates of thickness 75, 100 and 200 mm were evaluated by melting 10.0 mg samples of indium at 10°C min^{-1}. Typical curves for the melting of indium are shown in Fig. 7. The average area, peak height and width at half height at each plate thickness are shown in Fig. 8. The area, peak height and width at half height increased with decreasing plate thickness. The width at half height increased less with decreasing plate thickness than the peak height. Hence, by decreasing plate thickness, the sensitivity could be increased without a significant loss of peak resolution.

The greater sensitivity of thinner plates was thought to be due to their relative inability to supply heat to the sample area fast enough during melting, leading to a greater deficit in heat at the sample position. This leads to an increase in ΔT that would be greater in magnitude and last longer in thinner plates.

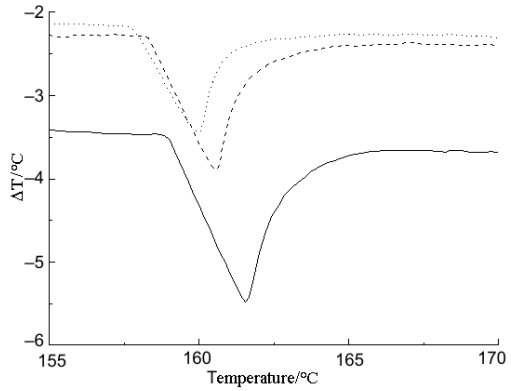

Fig. 7 Effect of inconel plate thickness on SR-DSC traces for the melting of 10 mg of indium —— 75 micron, – – – 100 micron, ····· 200 micron

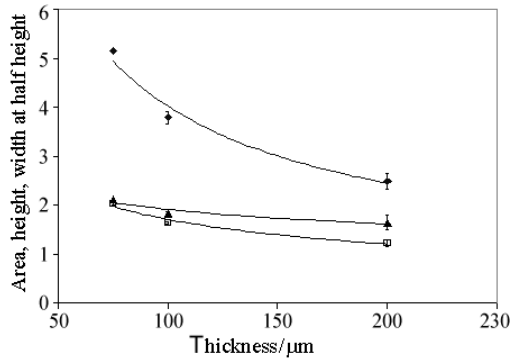

Fig. 8 Effect of inconel plate thickness on area, height and width of SR-DSC traces for the melting of 10 mg of indium. ◆ – area, □ – height, ▲ – width at 1/2 height

Four plate materials of different thermal conductivity (Table 1 [3]) were chosen and compared at a plate thickness of 100 μm. The four materials were inconel 600, constantan, nickel and silver. An indication of the sensitivity was obtained by melting 10 mg samples of indium. Typical curves for the melting of indium are shown in Fig. 9. The area, height and width at half height varied with thermal conductivity, Fig. 10. It was found that as thermal conductivity decreased, the peak area, peak height and peak width at half height all increased. However, the peak height was found to increase more markedly than peak width at half height, so by reducing thermal conductivity it was possible to increase instrument sensitivity without a significant trade-off in peak resolution.

Similar to the effect of plate thickness, it was considered that reducing the thermal conductivity reduces the flow of heat to or from the sample area, thus retarding the recovery of the sample area temperature.

The variation in calorimeter sensitivity with temperature was evaluated by dividing the heat of fusion per gram (Table 2) for four highly pure calibration materials, indium,

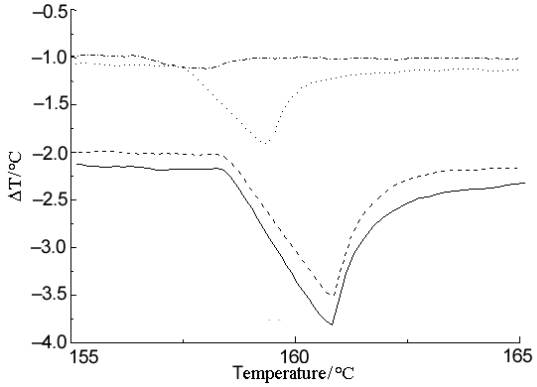

Fig. 9 Effect of plate material on SR-DSC traces for the melting of 10 mg of indium — inconel, – – constantan, ····· nickel, –·– silver

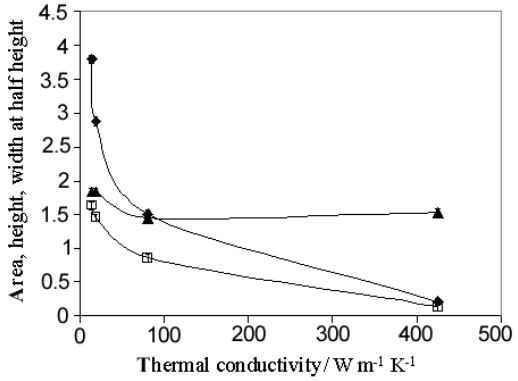

Fig. 10 Effect of thermal conductivity on area, height and width of SR-DSC traces for the melting of 10 mg of indium. ◆ – area, □ – height, ▲ – width at 1/2 height

tin, lead and zinc, $\Delta H/g^{-1}$ by the corresponding peak area per unit mass, i.e. $\Delta TS/g^{-1}$, where s is time, calculated from mass calibration results. The ratio produced is the heat of fusion per unit area of peak, *vs.* which is referred to here as the response, was plotted against temperature for inconel plates of different thickness in Fig. 11.

Table 2 Heat of fusion of metal standards

Material	Melting	Heat of fusion / J g^{-1}
Indium	156.60	28.57
Tin	231.97	60.60
Lead	327.50	23.10
Zinc	419.60	108.00

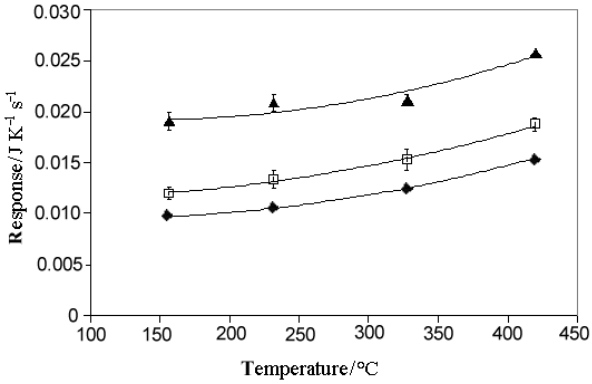

Fig. 11 Variation in response ratio with temperature for inconel plates. ◆ – 75 micron, □ – 100 micron, ▲ – 200 micron

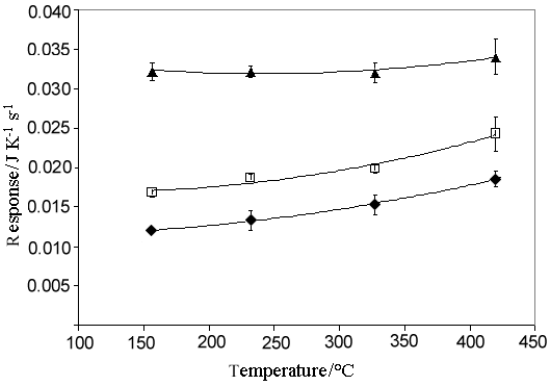

Fig. 12 Variation in response ratio with temperature for 100 micron plates made from different materials. ◆ – inconel, □ – constantan, ▲ – nickel

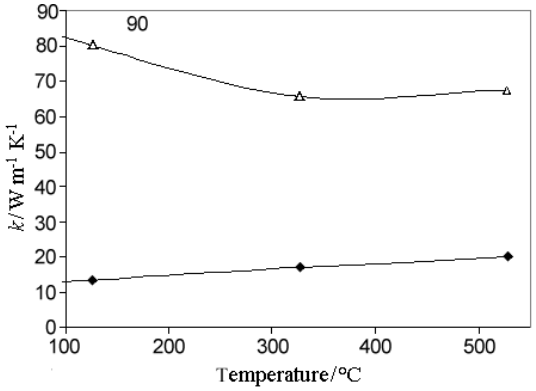

Fig. 13 Variation in thermal conductivity of inconel and nickel with temperature. ◆ – inconel, △ –nickel

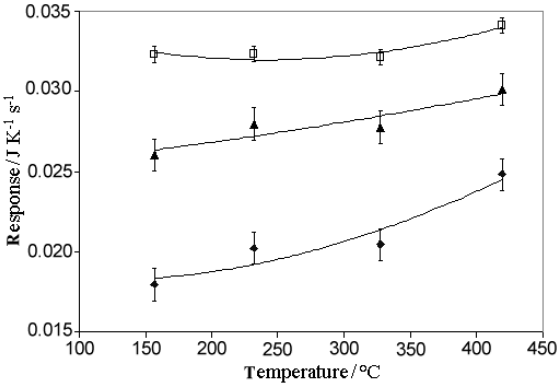

Fig. 14 Variation in response ratio with temperature for nickel plates ◆ – 50 micron, ▲ – 75 micron, □ – 100 micron

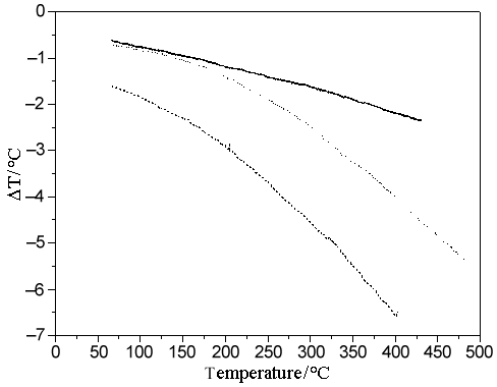

Fig. 15 Effect of plate material on baseline — silver, – – inconel, ···· nickel

The plots were found to be non-linear and the response ratio increased with temperature. The implication of this is that in order to measure enthalpy values by SR-DSC, a mass calibration must be carried out first, and the algorithm calculated can be used to convert the temperature difference between the reference and sample thermocouples, ΔT, into energy per unit time, i.e., J s^{-1}. Furthermore, the sensitivity of the calorimeter decreases with increasing temperature.

The variation of response ratio with temperature for plates of constant thickness (100 μm) made from inconel, constantan and nickel are shown in Fig. 12. The variation in response ratio with temperature was found to be consistent for inconel and constantan, although the plot for constantan was displaced up the *y*-axis, indicating that the constantan plate was less sensitive. However, the variation in response ratio with temperature for nickel did not follow the same trend. It was thought that this behaviour might have been due to variation in thermal conductivity with temperature for nickel being different to that for inconel (Fig. 13). The variation in response ratio with temperature for nickel plates of different thickness is shown in Fig. 14. It was

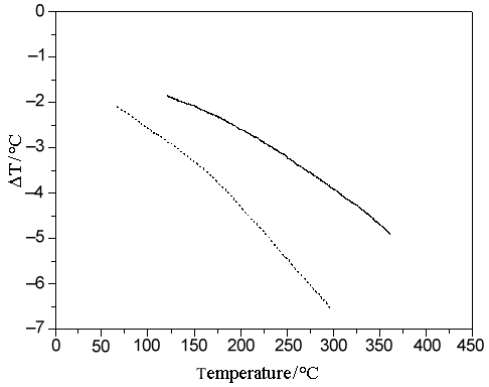

Fig. 16 Effect of inconel plate thickness on baseline – – 75 micron, — 200 micron

found that thinner plates followed the trend observed for inconel plates. It was considered that the sensitivity of the 100 μm nickel plate was so low that considerable errors were introduced, and that in fact, nickel plates followed the same variation in ΔH/A with temperature as inconel and constantan plates.

The similarity in the variation of $\Delta H/\Delta Ts$ with temperature for plates of different materials was thought to be due to the dominance of heat loss by emissivity over the thermal conductivity at elevated temperature.

In SR-DSC, the baseline is established by subtracting the reference temperature from the sample temperature, and as such is determined by the temperature gradient across the plate. The temperature gradient across the plate at all temperatures was expected to depend upon the thermal conductivity, k, according to,

$$T_{\text{sam}} - T_{\text{ref}} = \frac{Q}{t}\frac{d}{ka} \tag{1}$$

where T_{ref} is reference temperature, T_{sam} is sample temperature, Q/t is heat flow per second, d is distance between T_{ref} and T_{sam}, a is cross-sectional area and k is thermal conductivity.

The baseline produced by 100 μm plates of inconel, nickel and silver were analysed at a heating rate of 10°C min^{-1} (Fig. 15). It was found that the material of lowest thermal conductivity, inconel, had the most pronounced baseline slope, and the material of highest thermal conductivity, silver, the least sloped baseline. However, as can be seen, the baseline slope does not reflect the changes in thermal conductivity occurring in the plates. It was considered that heat loss from the plate surfaces (emissivity) affected the baseline. Figure 16 shows that thinner plates produce more sloped baselines, which was probably due to the dominance of surface emissivity in thin plates.

In the case of the 75 μm thick inconel plate, it was possible to detect the melting of 120 μg of indium above the noise level. The fluctuation in the baseline was at worst ± 0.05 K. It was considered that the baseline noise level could be reduced by securing the DSC plate to prevent movement, improving the furnace temperature stability and by controlling the environment around the furnace, e.g. using a water jacket.

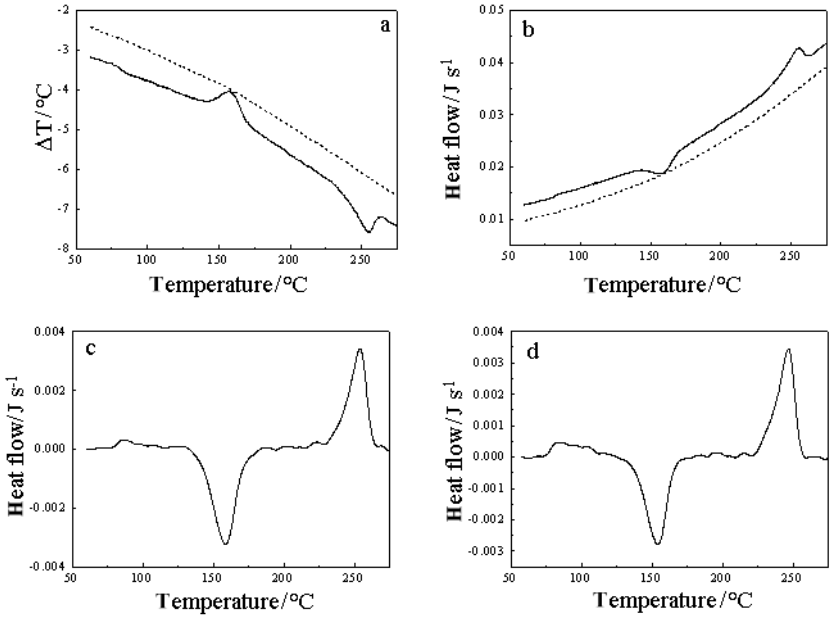

Fig. 17 Manipulation of SR-DSC data for the melting of 25 mg of PET on 75 micron inconel plate, a – raw SR-DSC data — sample – – baseline, b – SR-DSC data converted to J s^{-1} — sample – – baseline, c, baseline algorithm subtracted, d – actual baseline data subtracted

Correction of data to account for sensitivity and baseline variations

Although the instrument sensitivity and baseline was found to vary with temperature, the variations were highly reproducible, hence the baseline can be subtracted and the variation in calorimeter sensitivity can be corrected by means of an algorithm developed from the variation of $\Delta H/\Delta Ts$ with temperature. The procedure for data correction is described as follows for the thermal analysis of 10 mg amorphous PET at 10 K min^{-1}.

Amorphous PET, prepared by quenching from the melt in contact with a cold aluminium bar, was heated from 323 to 543 K at a heating rate of 10 K min^{-1}, and the results are shown in Fig. 17a, with a baseline which was recorded afterwards. The *y*-axis was converted from temperature difference, ΔT in °C, to heat flow in J s^{-1} by means of an algorithm of the variation in $\Delta H/\Delta Ts$ with temperature (Fig. 17b). This calibrates ΔT to its associated enthalpy change and corrects for variations in calorimeter sensitivity with temperature. Further to this the baseline can be subtracted by means of an algorithm of the baseline (Fig. 17c) or actual baseline data (Fig. 17d). Subtraction of a baseline algorithm has the advantage of being noise free data, whereas actual data is more representative of the true baseline at the early stages of an

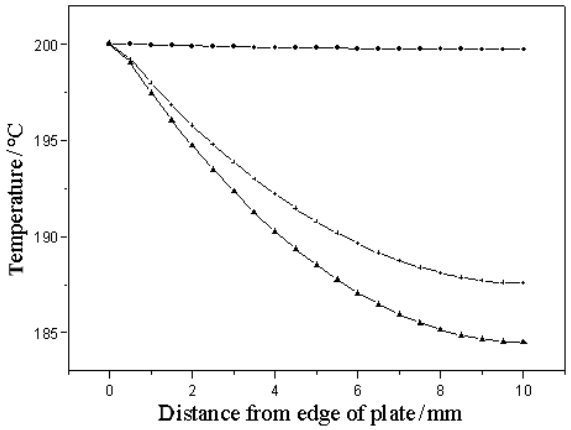

Fig. 18 Simulated temperature gradient across a thermal plate. ● – silver, + steel, ▲ – inconel

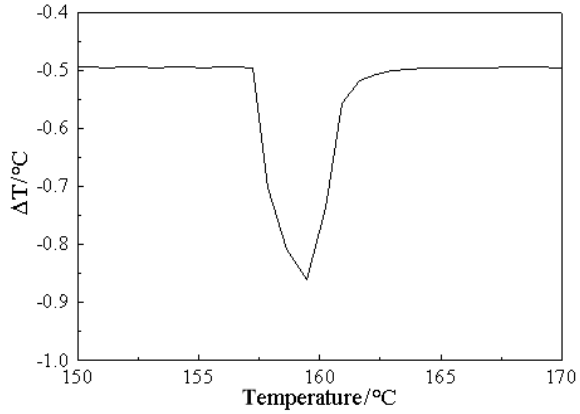

Fig. 19 Simulation of the melting of indium on an inconel plate

experiment where the baseline is not quite at equilibrium conditions, hence a clearer glass transition is observed in Fig. 17d.

Finite element analysis of heat flow across a thermal plate

Finite element analysis was used to investigate the effect of material choice, thickness and geometry on the performance of SR-DSC thermal plates. The following equation was used to calculate the temperature at each node on the plate,

$$T - T' = \frac{Q}{t}\frac{d}{ka} \tag{2}$$

where T and T' are the temperatures of two nodes on the plate.

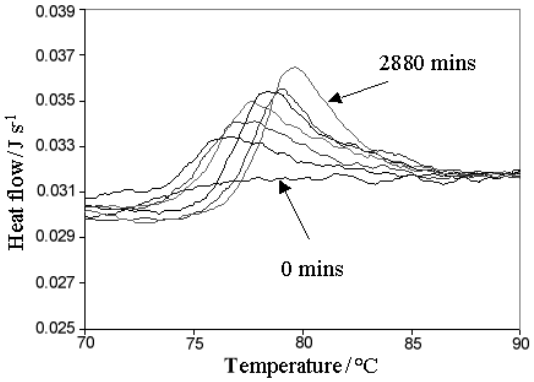

Fig. 20 SR-DSC traces of the physical ageing of PET

In order to determine the effect of plate material on the performance of the plate, the density, heat capacity and thermal conductivity of each material, and their variation with temperature, were defined. These values were used to determine α, which is a measure of heat flow, using the equation,

$$\alpha = \frac{k}{\rho C_p} \tag{3}$$

where ρ is density, C_p is heat capacity and k is thermal conductivity.

The heat flow across thermal plates of silver, steel and inconel was simulated, with the temperature at the edge of the plate set at 200°C. The temperature gradient across the plate differed for each material (Fig. 18). Using silver, a very small temperature gradient developed, indicating that heat was readily conducted across the plate. In section 'Results and discussion' it was found that silver was a poor choice of material for a thermal plate, as good heat flow reduces the magnitude of the response to a thermal transition. Larger temperature gradients were developed using inconel and steel, which are poor thermal conductors, consistent with the results shown the abovementioned section 3. However, at this stage it is not clear whether a or k is the dominant factor in obtaining good calorimeter sensitivity, and this will be the subject of further investigation.

The melting of a sample of indium on a 100 μm inconel plate was also simulated. For the software to allow heat flow from the plate to the sample, a contact pair had to be defined. This ensured that the very bottom of the sample, in contact with the plate, was the same temperature as the plate at the point of contact. To successfully simulate melting, the latent heat, solidus temperature and liquidus temperatures were defined. The sample temperature was taken from the central node of the plate, and the reference temperature obtained from a node half way between the edge and the centre of the plate. Figure 19 shows how ΔT changes with temperature as the sample is heated. The melting of indium can be seen as a sharp peak. The size of the response and the baseline cannot be directly compared to practically obtained results, due to

emissivity effects, i.e. loss of heat from the surface of the plate to the surrounding environment. However, even without this correction, the analysis can be used to detect trends in sensitivity with plate thickness and material choice, which will be the subject of future work.

The physical ageing of PET

The physical ageing of amorphous PET was carried out at 338 K to demonstrate the ability of the SR-DSC to measure such a low energy transition, compared to power-compensation DSC [4]. The polymer was rapidly quenched as described in section 'Correction of data', and the molecular conformation of the liquid is frozen. At this stage, the polymer chains in the glass have a higher energy conformation than at equilibrium. However, the polymer retains some mobility and can relax over time to the equilibrium conformation, and this process is known as physical ageing [5].

Amorphous PET (25 mg) was held at 338 K for periods up to two days. At certain times, the temperature would be raised at 10 K min^{-1}, through the glass transition, to 368 K, and back to 338 K at 2.5 K min^{-1}. This process was immediately repeated to obtain the unaged glass transition. The unaged glass transition is subtracted from each physical ageing peak, and the remaining area is associated with the enthalpy of physical ageing. SR-DSC curves of PET at various stages of physical ageing are shown in Fig. 20. The changes caused by physical ageing are clearly visible, and the results are at least as good as those for power-compensation DSC reported in the literature [4].

Conclusions

It was concluded that acceptable sensitivity could be obtained from the SR-DSC constructed in this study. The best sensitivity was achieved using the thinnest plate made from the material of lowest thermal conductivity, which restricted the recovery of equilibrium heat flow following a thermal transition. FEA of the thermal plate can be used to model heat flow changes during melting transitions.

References

1 W. Hemminger and G. Höhne, Calorimetry Fundamentals and Practice, Verlag Chemie, Weinheim 1984 p. 102.
2 W. Hemminger and G. Höhne, Calorimetry Fundamentals and Practice, Verlag Chemie, Weinheim 1984 p. 109.
3 F. W. Incropera and D. P. DeWitt, Fundamentals of Heat and Mass Transfer, 4th Ed, John Wiley & Sons, New York 1996 p. 827.
4 N. A. Bailey, J. N. Hay and Price DM, TCA, 367 (2001) 425.
5 A. K. Kovaks, Fortschr. Hochpolm Forsch, 3 (1963) 394.